*Article*

# Aminated Graphene Nanomesh: Theoretical and Experimental Insights into Process of Decorating, Topology and Electron Properties

Olga E. Glukhova [1,2,*], Maxim K. Rabchinskii [3], Svyatoslav D. Saveliev [3], Demid A. Kirilenko [3] and Pavel V. Barkov [1]

1   Institute of Physics, Saratov State University, Astrakhanskaya 83, 410012 Saratov, Russia
2   Laboratory of Biomedical Nanotechnology, I.M. Sechenov First Moscow State Medical University, Bolshaya Pirogovskaya Street 2-4, 119991 Moscow, Russia
3   Center of Nanoheterostructures, Ioffe Institute, Politekhnicheskaya Street 26, 194021 Saint Petersburg, Russia
*   Correspondence: glukhovaoe@info.sgu.ru; Tel.: +7-8452-514562

**Abstract:** The physicochemical nature of the amino group $NH_2$'s landing on the basal plane of the graphene and on the edge atoms of the graphene nanomesh was revealed. The mechanism of covalent binding between the $NH_2$ groups and the carbon atoms of the graphene and the GNM was discovered in silico by the SCC DFTB method. The maximum amount ratio of the amino groups to carbon atoms equaled 4.8% for GNM and 4.6% for the basal plane. The established values of the concentration and the trend of change in the work function of electrons are experimentally confirmed.

**Keywords:** graphene; graphene nanomesh; aminated graphene nanomesh; amino groups; functionalization; in silico

## 1. Introduction

Graphene nanomesh (GNM) is one of the graphene nanomaterials that continue to develop rapidly [1–3]. GNM has adjustable electronic properties including a tuning band gap, a high specific surface area and a unique topology [4]. Such 2D-nanomaterials with holes of different nanometer sizes are widely applied in electronics, gas nanosensors, membrane filtration, catalysis as well as for energy storage and conversion [5–9]. This material is unique since its properties can be tuned in the result of certain functionalization. For example, on the basis of GNM decorated with single-stranded DNA, a sensor device was designed with fast response and recovery for detecting different substances including carbon acids, aldehydes, organophosphates and explosives [10]. Based on a N-doped GNM, a highly efficient electrochemical sensor was successfully developed to determine residual amounts of organophosphate pesticides including methylparation [11]. Aminated GNM can be effectively used as a metal-free catalyst for oxygen-reduction reactions [12]. Functionalization by silicon or nitrogen makes GNM a promising material for a design of lithium-ion battery electrodes and supercapacitors [13]. Xu et al. found that the performance parameters of nitrogen-doped GNM electrodes are significantly improved in comparison to pure GNM; a battery with such an electrode demonstrates stable operation with capacity retention for 6000 cycles [14]. The GNM is in general decorated with oxygen-containing groups [15–19]. It is shown that the presence of oxygen-containing groups leads to an increase in a GNM-specific capacity due to the increased Faraday reactions leading to an additional charge accumulation [19]. The application of GNM with oxygen-containing groups is also promising for sensors application. Earlier it was shown that graphene oxide demonstrates excellent sensor parameters including increased sensitivity to gases such as $NO_2$, $NH_3$, CO, ethanol, $H_2O$, trimethylamine, HCN and dimethylmethylphosphonate [20]. Such material is a prospect element for chemoresistive sensors [21].

Equally important for practical purposes is the functionalization of the graphene's basal surface accompanied with a formation of $sp^3$ bonds in carbon atoms. Since $NH_2$ is an electron-withdrawing group, decorating graphene with amine groups changes its electronic structure, in particular, increasing conductivity and tuning the electron work function [22]. At present, aminated graphene is considered as a promising material for various applications in photovoltaics, gas and biosensors, for drug delivery and for the synthesis of new composites [23–26]. Various strategies for amine functionalization of graphene are used. For example, amine groups are attached via plasma functionalization [27].

It was shown experimentally that amino groups attach to edge atoms as well as to a basal surface. However, it remains unclear which landing is preferable and how exactly it occurs, what is the topology of the groups' arrangement, which of cis- or trans-configuration is beneficial. This hinders practical approaches for engineering the topology of amine groups on graphene. To approach this issue, in silico approaches are required. Note that many papers are devoted to simulation of graphene nanostructure functionalization by different topologies [28–32]. One of the important points here is a correct determination of functional groups' landing sites. The paper [28] is devoted to a comprehensive analysis of different approaches for the modeling of graphene functionalization by quantum-chemical methods: empirical, semiempirical and DFT. Models of functionalized graphene obtained by the DFT approach are also shown in [29–31]. Empirical approaches to graphene–polymer nanocomposite functionalization simulation [32] and finite-element methods for exploring new properties of functionalized graphene nanoplates [33] are also in demand. Some patterns of graphene functionalization by different groups are identified. For example, it is found that the most often met oxygen-containing groups at the graphene surface are epoxy (C-O-C), phenolic hydroxil (-OH), carboxyl (-COOH) and other carbonyl groups (C=O) distributed over the surface of graphene sheets. Herewith, carboxyl groups are located mostly at the edges while phenolic hydroxil and epoxy are located at the basal plane [34–36]. Other widely spread groups contain nitrogen, sulfur, fluorine and other atoms [37–39].

This work is devoted to exploring the physicochemical nature of the functionalization of a graphene's basal plane GNM circle with amino groups, in order to establish a landing-group topology, its concentration and influence on the electronic structure.

## 2. Materials and Methods

### 2.1. Computational Details

The modeling was performed by the self-consistent charge density functional tight-binding (SCC DFTB) [40] method realized in dftb+ [41]. A supercell of the GNM represented the monolayer graphene of 186 carbon atoms with a circle hole of 1.2 nm in diameter. Optimization was performed in periodic box with lattice vectors of $2.46 \times 2.55$ nm. The basal plane of graphene represented the GNM of the same sizes but without a hole. Dispersion interaction was taken into account by the application of the Lennard–Jones potential with Universal Force Field (UFF) parameters. The sampling of the Brillion zone was performed by the Monckhorst–Pack scheme with $6 \times 6 \times 1$ mesh. The electron temperature was equal to 300 K. The search of the ground state was performed by the conjugate gradient method using lattice vectors and atom coordinates as the variable parameters.

### 2.2. Materials Synthesis

All the studied functionalized graphenes were synthesized via liquid phase modification of the initial graphene oxide (GO) purchased from Graphene Technologies, Ltd. (Moscow, Russia, www.graphtechrus.com, accessed on 30 July 2022). During the GO synthesis, sonication was excluded to prevent the disruption of flakes, achieving their mean lateral size of 10–200 μm.

C-ny graphene was synthesized according to the method described in Ref. [42]. In brief, 30 mL GO aqueous suspension of 0.3 wt.% of the concentration was poured into a Teflon reaction vessel and mixed with $Na_2SiO_3$ powder (Merck, US) while stirring to reach

pH = 9. The pH values of the suspensions were evaluated with a Fisher Scientific Accumet Basic AB15 pH meter (Thermo Fisher Scientific, Waltham, MA, USA). The acquired reaction mixture was heated at $T$ = 80 °C for 48 h in the air while stirring. Afterwards, it was cooled down to room temperature and purified via five cycles of centrifugation (Sigma S-16 centrifuge, Roedermark, Germany), for 15 min each, with an acceleration of 18,200 g and sequential rinsing of the obtained sediment at distilled water (30 mL).

The set of aminated graphenes was synthesized using the Leuckart reaction [43], using C-ny graphene or GO as an initial substrate. Holey Am graphene, denoted hereinafter as Am#1, was acquired by pouring C-ny aqueous suspension, of 15 mL volume at 0.8 wt.%, into a Teflon reaction vessel with the subsequent addition of 50 mL of $CH_3NO$ (Merck, Darmstadt, IN, USA). The acquired reaction mixture was heated at $T$ = 125 °C for 72 h with the vessel being connected to the reflux condenser. Afterwards, the suspension was cooled down to room temperature and the synthesized rGO-Am was copiously washed with deionized water (3 cycles) and isopropyl alcohol (3 cycles) using a glass filter of 40 μm of pore size. To synthesize the pristine Am graphene (Am#2), the GO aqueous suspension instead of the C-ny graphene was treated in otherwise identical conditions. Finally, the overfilled Am graphene (Am#3) was synthesized by the same synthesis protocol but raising the temperature to $T$ = 165 °C.

### 2.3. Materials Characterization

The present and relative concentration of amine groups along with other nitrogen- and oxygen-containing moieties in the synthesized amine graphenes was examined by the means of X-ray photoelectron spectroscopy (XPS). The survey, C 1*s*, and N 1*s* X-ray photoelectron spectra were collected using the NanoPES experimental station at the Kurchatov Synchrotron Radiation Source (National Research Center Kurchatov Institute, Moscow, Russia). The ESCA module (SPECS) equipped with XR-MF microfocus X-ray source (Al K$\alpha$, 1486.61 eV) and Phoibos 150 analyzer was used. The spectra were calibrated with respect to the Au 4f7/2 line (84.0 eV). Prior to the measurements, all samples were placed at a chamber evacuated down to the pressure of P = $10^{-9}$ Torr for 6 h to remove all possible adsorbates. No heating was applied to prevent the changes in the composition of oxygenic moieties in the GO. XPS survey spectra were measured with the energy step of 0.5 eV, while for the C 1*s* and N 1*s* core-level spectra, this value was 0.05 eV.

For each studied material, the X-ray photoelectron were collected in four different areas of the sample with the subsequent averaging for further processing. CasaXPS software (Version 2.3.16Dev52, Casa Software Ltd., Teignmouth, United Kingdom) was applied for the deconvolution of the acquired C 1*s* and N 1*s* X-ray photoelectron spectra with a subsequent quantification of the relative concentration of the carbon and nitrogen atoms at different states. All the spectra were fitted with a Shirley background. For the C 1*s* deconvolution, a set of one asymmetric Doniach–Sunjic function (DS0.15,150; GL90) and five symmetric Gaussian–Lorentzian functions of a 30–70% ratio (GL(30)) were applied. For the N 1*s* deconvolution, four symmetric Gaussian–Lorentzian functions of a 30–70% ratio (GL(30)) were applied.

For the XPS measurements, all the samples were prepared on the Si wafers (p$^{++}$) by the drop-casting of 75 μL of the isopropyl suspensions, $5 \times 10^{-1}$ wt.% of concentration, with the subsequent drying at room temperature (ca. 25 °C) for 3 h.

To examine the work function values of the synthesized materials, the SE cut-off spectra were acquired at the excitation energy of $hv$ = 130 eV at the Russian–German beamline of electron storage ring BESSY-II at Helmholtz-Zentrum Berlin (HZB), using the ultrahigh vacuum experimental station [44]. To calculate the WF values, the following equation was used:

$$e\Phi_m = hv - (E_F - E_{SEC}) \tag{1}$$

where $hv$ = 130 eV is the energy of the photons, $E_F$ and $E_{SEC}$ are the positions of the Fermi level and the cut-off threshold, both represented in the kinetic energy scale [45].

The set of microscopic methods was applied to analyze the crystal structure and morphology of the synthesized Am graphenes. TEM images and ED patterns were acquired from the GO and the Am graphene platelets deposited from the aqueous and isopropyl suspensions, of $5 \times 10^{-5}$ wt.% of concentration, on the surface of the TEM Cu grids (400 Mesh), using a Jeol JEM-2100F microscope (Jeol, Tokyo, Japan) with a point-to-point resolution of 0.19 nm at an accelerating voltage of 200 kV.

## 3. Results

### 3.1. In Silico Functionalization of GNM

The process of the GNM functionalization by amino groups was performed by the original methodic, which allows the unveiling of the stereochemical configuration and spatial distribution of any functional group on the edges of the GNM holes. Feasibility of this methodic was demonstrated in one of our previous works, exhibiting the theoretical examination of the structure and electrophysical properties of GNM decorated by the carboxyl groups, which results fully coincided with experimental findings [46]. For the case of amine groups covalently attached to the edges of nanoholes, the methodic was employed as follows: (1) an optimization of a supercell atomic structure and calculation of electron charge density distribution over atoms; (2) an identification of the atom with a maximum amount of excess charge and the binding of amino group to this atom; (3) a passivation of the neighbor edge atom and a reoptimization of the supercell. This process continued while all the edge atoms near the nanohole were not functionalized. Figure 1 shows the supercell with the circle hole in two angles: top and side view. Down the arrow, there is the supercell with the one attached group of $NH_2$ (marked with the number "1"), and next to it is there is a color map of the electron charge density distribution over the atoms; next, on the arrow on the right side of the figure, there are two different configurations of the attached $NH_2$ group (marked with the number "2")—cis and trans.
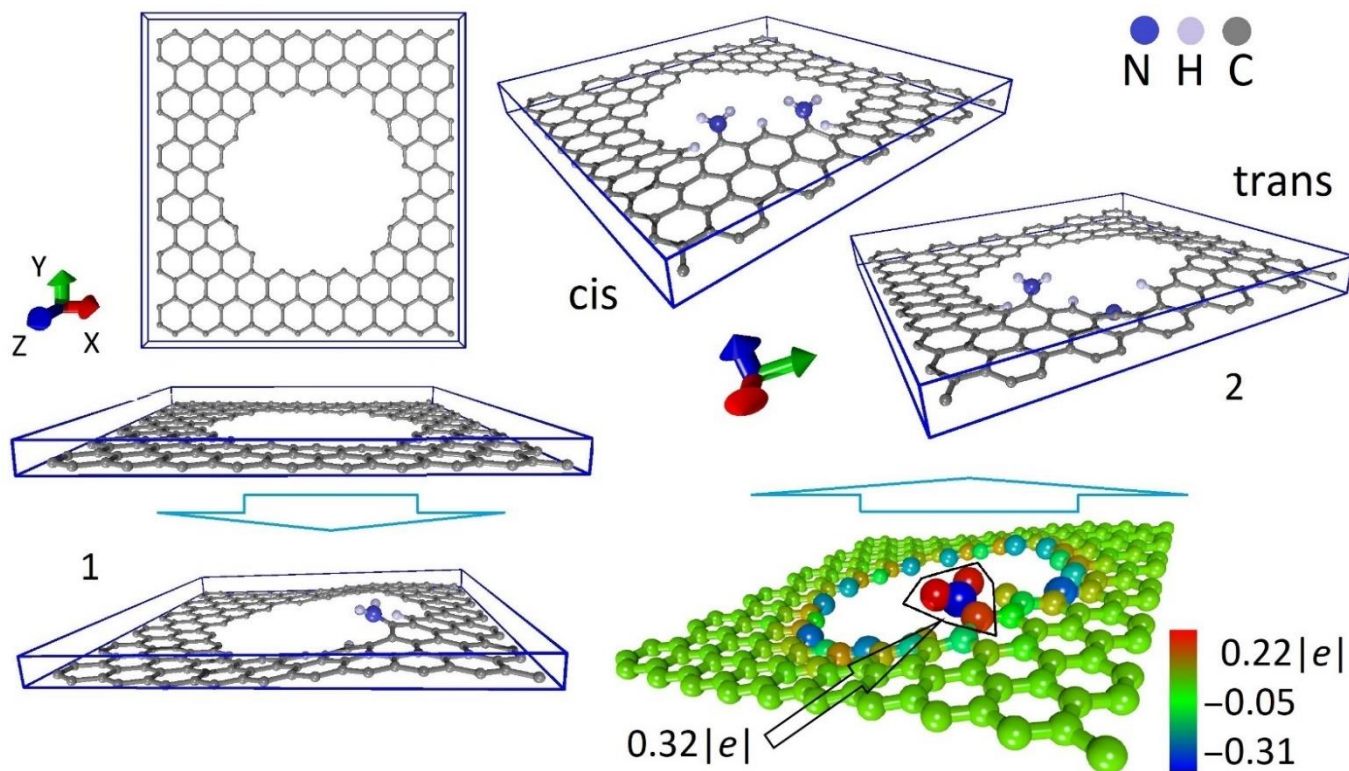


**Figure 1.** Supercells of pure GNM and functionalized by one and two amino groups (cis- and trans-configuration), periodic box corresponds to blue lines; distribution of electron charge density in the case of one group landing (in in electron charge units).

As it is seen from Figure 1, initially the GNM was a perfectly flat structure. An addition of the $NH_2$ groups lead to a noticeable curvature of the supercell's atomic mesh: the $NH_2$ group seemed to "pull" part of the atomic mesh above the plane—up in the direction of the Z axis. After the attachment of one $NH_2$ group, part of its charge flew to the graphene. As shown in Figure 1, there is a lack of an electron charge of $0.32|e|$ on the $NH_2$ molecule. There is also an excess charge on almost all the atoms of the basal surface (marked with a green-blue shade). After adding a second group of $NH_2$, two almost identical energy variants appeared. In both cases, a bunch of C-$NH_2$ atoms also had an insufficient electronic charge, but in this case, it equaled to $0.28 \pm 0.01|e|$ regardless of the cis- or trans-configuration.

The pure GNM demonstrated a small energy gap of 0.04 eV and a Fermi level of −5.02 eV. After the addition of an amine group and two hydrogen atoms, the gap increased to 0.12 eV and the Fermi level shifted to −4.90 eV. The heat of formation ΔE, calculated as the difference between the energy of the final structure and the energies of the isolated initial structures (GNM, hydrogen and $NH_2$ groups) was −16.89 eV. The negative value indicated that the addition of an $NH_2$ group was an energetically favorable process. Further, the procedure for the $NH_2$ group attachment was performed according to the scheme described above. At each step, the amino groups were attached in two configurations, cis and trans, that were energetically favorable. In both cases, the addition of each new amino group led to a certain degree of the graphene layer deformation. The continuation of the gradual addition of amine groups from three to eight is shown in Figure 2a. Table 1 shows the energy parameters reflecting the appearance of each new amine group at the edge atoms of the GNM hole: heat of formation ΔE, Fermi level $E_F$ and the value of the energy gap $E_{gap}$ for different numbers of the $NH_2$ groups and, accordingly, their concentration $C_{NH2}$ relative to the number of carbon atoms. Figure 2b shows the top view of the supercells with the full functionalization of the nanohole by the $NH_2$-groups for the two configurations cis and trans. It can be seen that nine $NH_2$ groups alternate with nine hydrogen atoms on the nanoholes' atoms (Figure 2b shows the top view). The distribution of the electron charge density over the atoms was also calculated (Figure 2b). The maximum excess charge is observed on the nitrogen atoms (−0.37 e), the maximum lack of electron density of 0.21 e corresponds to the hydrogen atoms, and the graphene atoms have a small excess of charge.

**Table 1.** Energetic parameters of a functionalized GNM.

| NH$_2$/H | C$_{NH2}$, % | ΔE, eV | E$_F$, eV | E$_{gap}$, eV | ΔE, eV | E$_F$, eV | E$_{gap}$, eV |
|---|---|---|---|---|---|---|---|
| | | | Cis | | | Trans | |
| 2/3 | 1.07 | −11.14 | −4.73 | 0.11 | −11.04 | −4.75 | 0.10 |
| 3/5 | 1.61 | −16.65 | −4.65 | 0.14 | −16.75 | −4.67 | 0.16 |
| 4/5 | 2.15 | −5.30 | −4.52 | 0.08 | −5.28 | −4.53 | 0.09 |
| 5/7 | 2.69 | −16.58 | −4.44 | 0.03 | −16.60 | −4.45 | 0.04 |
| 6/7 | 3.22 | −5.31 | −4.34 | 0.07 | −5.29 | −4.34 | 0.09 |
| 7/8 | 3.76 | −10.91 | −4.21 | 0.25 | −10.86 | −4.23 | 0.26 |
| 8/9 | 4.30 | −10.85 | −4.07 | 0.23 | −10.83 | −4.07 | 0.27 |
| 9/9 | 4.84 | −5.21 | −3.88 | 0.26 | −5.18 | −3.88 | 0.26 |

Thus, for the considered configuration of GNM with 1.2 nm in diameter, the maximum concentration of amino groups was equal to 4.84%.

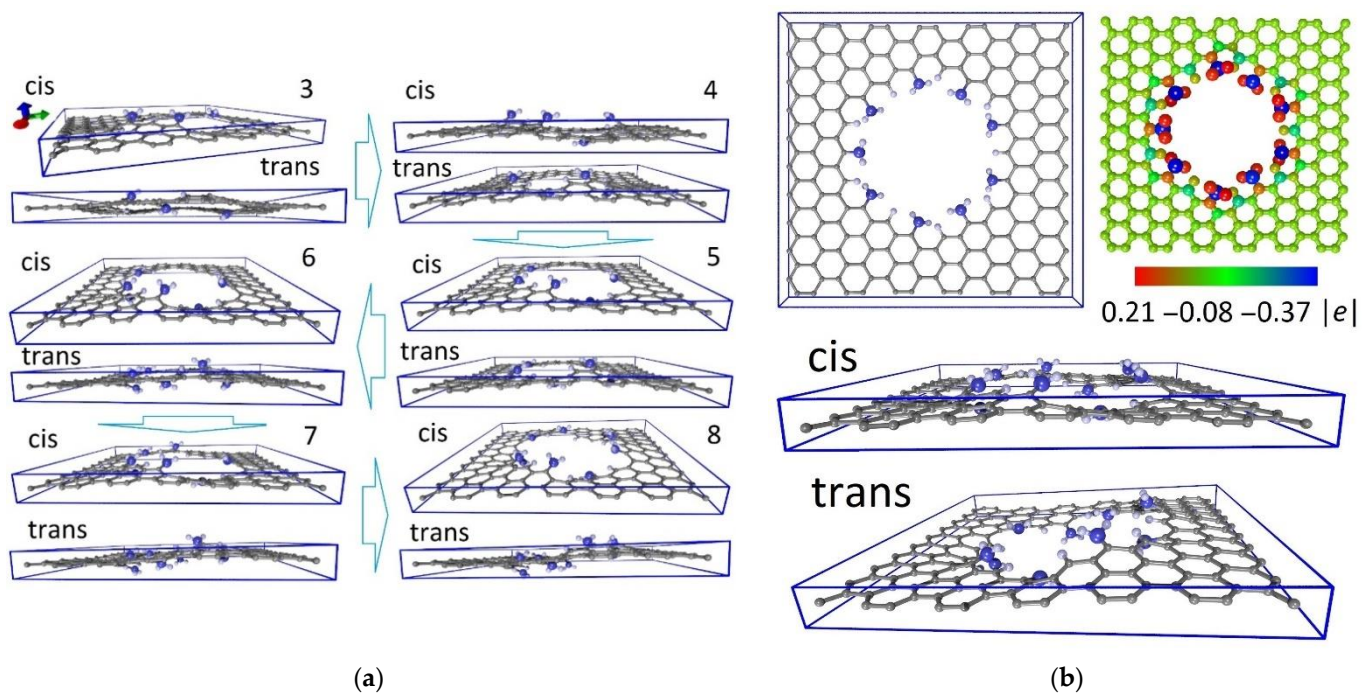**Figure 2.** The supercell of GNM decorated with $NH_2$ groups: (**a**) consequent attachment of 3rd–8th amino groups of two configurations cis and trans; (**b**) full functionalization of nanohole and the distribution of the electron charge density over atoms.

### 3.2. In Silico Functionalization of Graphene's Basal Plane

Further similar studies were performed for the graphene's basal plane. Unlike the GNM, a density of electron charge is the same for all atoms, so the one atom in the center of the graphene was chosen for the landing of a first amino group. A fragment of the structure obtained after optimization is shown in Figure 3 (marked with the number "1"). The heat of formation was −0.57 eV; thus, the formation of a covalent bond between the amine group and the basal plane of graphene is energetically favorable. Therefore, the functionalization of the graphene by the amine groups is a natural process realized under normal physical conditions. The next step was to analyze a distribution of an electron charge density over the atoms of the supercell with one attached amine group. The second amine group was attached to the atom with an excess charge. As noted in Section 3.1, there are two configurations, cis and trans, that can be attached. However, unlike the GNM, in this case only the staggered landing option is energetically favorable—when one amine group is located above the plane and the other is located below it. This can be seen in Figure 3 (marked with the number "2"). According to the same algorithm based on the detection of an atom with an excess charge, the following third, fourth, fifth, sixth and seventh amine groups were attached, as shown in Figure 3. After each new binding, the supercell was reoptimized, which proved physically justified and as close to real results. Such an in silico approach allows us to reveal the mechanism of the graphene's functionalization, in particular by the amine groups.

The energy parameters of the graphene during functionalization are presented in Table 2. The heat of formation is negative, as in the case of the GNM, but it is significantly less in absolute value. This is predetermined by the fact that the atoms of the basal surface of the graphene are in the state of sp2 hybridization, while the atoms of the GNM are in sp hybridization. However, the main conclusion at this stage is the fact that covalent binding of the amine groups to the basal graphene is energetically advantageous, which means it is quite feasible in practice. At the same time, it should be noted that the addition of one group already shifts the Fermi level by one tenth of an electron volt in the direction of zero, and this trend can be traced with further functionalization by the amine groups.

The addition of only one amino group leads to the opening of an energy gap in the band structure up to several hundredths of an electron volt. Thus, already at the concentration of groups less than 0.35%, a small gap opens in the zone structure of the graphene and increases with the addition of five or more groups.
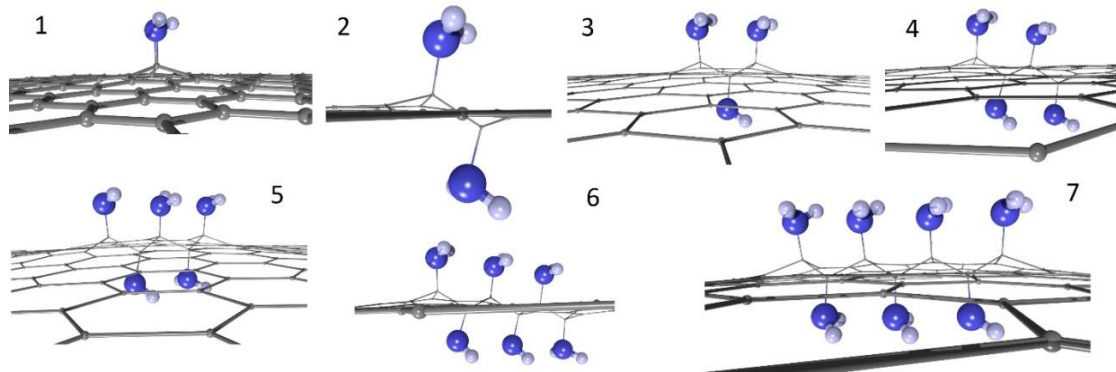


**Figure 3.** A fragment of the graphene's basal plane functionalized with 1–7 amino groups.

**Table 2.** Energetic parameters of a functionalized graphene.

| NH$_2$ | C$_{NH2}$, % | $\Delta$E, eV | E$_F$, eV | E$_{gap}$, eV | NH$_2$ | C$_{NH2}$, % | $\Delta$E, eV | E$_F$, eV | E$_{gap}$, eV |
|---|---|---|---|---|---|---|---|---|---|
| 0 | - | 0.00 | −4.61 | - | 4 | 1.39 | −1.95 | −4.48 | 0.04 |
| 1 | 0.35 | −0.57 | −4.51 | 0.03 | 5 | 1.74 | −1.48 | −4.44 | 0.04 |
| 2 | 0.70 | −2.21 | −4.50 | 0.03 | 6 | 2.08 | −1.72 | −4.45 | 0.05 |
| 3 | 1.04 | −1.35 | −4.47 | 0.03 | 7 | 2.43 | −1.31 | −4.44 | 0.05 |

As noted above, the landing of the groups was performed based on the analysis of the electron charge density distribution over atoms. This approach was implemented for the first seven groups, after which it was discovered that there are two atoms with excess charge. In this regard, two options for further graphene functionalization were considered. Figure 4 shows a fragment of the graphene plane with seven NH$_2$ groups and the following two variants of an eighth group landing. In one of the landing options 8-2, all subsequent amine groups land in a zigzag direction that is clearly seen in Figure 4. All the previous seven groups, as in the case of option 8-2, landed exactly in the zigzag direction and only when the eighth group landed, two alternative ways of subsequent functionalization arose. In the option 8-2, the amine groups are equally clearly located on both sides of the graphene. Option 8-1 demonstrates a deviation from the zigzag "trajectory". The subsequent landing of the groups followed two trajectories. Figure 4 shows two options for the attachment of the 11 groups. The graphene atoms to which the groups are attached are marked in yellow, the N-atoms of the amine groups located on top are marked in blue, and the N-atoms of the groups under the graphene plane are marked in green.

The next step was to attach the next 12th group. Figure 5 shows the configurations before and after optimization for both landing options. As a result of optimization, it was found that the landing of the 12th amine group led to a break of the graphene atomic mesh with the formation of a nanohole. In fact, 11 is the maximum possible number of amino groups that can be attached to the graphene surface; the next landing of the amine group forms the GNM. In the first option (12-1), the graphene destruction was accompanied by the elimination of several amine groups and hydrogen atoms with a simultaneous formation of an ammonia molecule. The carbon atoms to which the amine groups were attached (marked in yellow) partially lost amino groups, partially eliminated. In the second case (12-2), the graphene destruction looked like a clear cut in the zigzag direction. Carbon atoms remained in the graphene, and the amine groups were not eliminated. Table 3 shows the energy parameters of the landing process for the 8th–12th amino groups. First of all, there is a tendency to shift from the Fermi level in the direction of the zero electron volts

as the number of amine groups increases for both variants of their planting. Before the landing of the 11th group, the heat of the formation was negative and only when the 12th group was planted, the heat of the formation became positive. As noted above, there was a break in the graphene mesh and an elimination of several amine groups that affected the energy parameters. However, the second option of the landing was favorable since $\Delta E < 0$, although it led to the cutting of the graphene sheet.



**Figure 4.** Two landing options of 8th–11th amine groups to basal plane of graphene. Graphene atoms to which the groups are attached are marked in yellow, N-atoms of amine groups located on top are marked with blue, and N-atoms of groups under the graphene plane are marked with green.
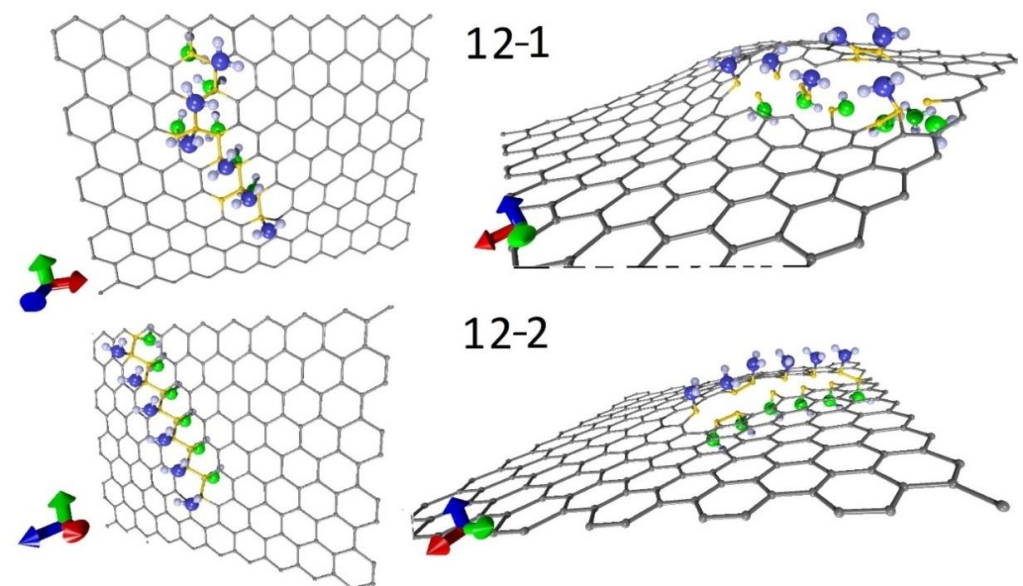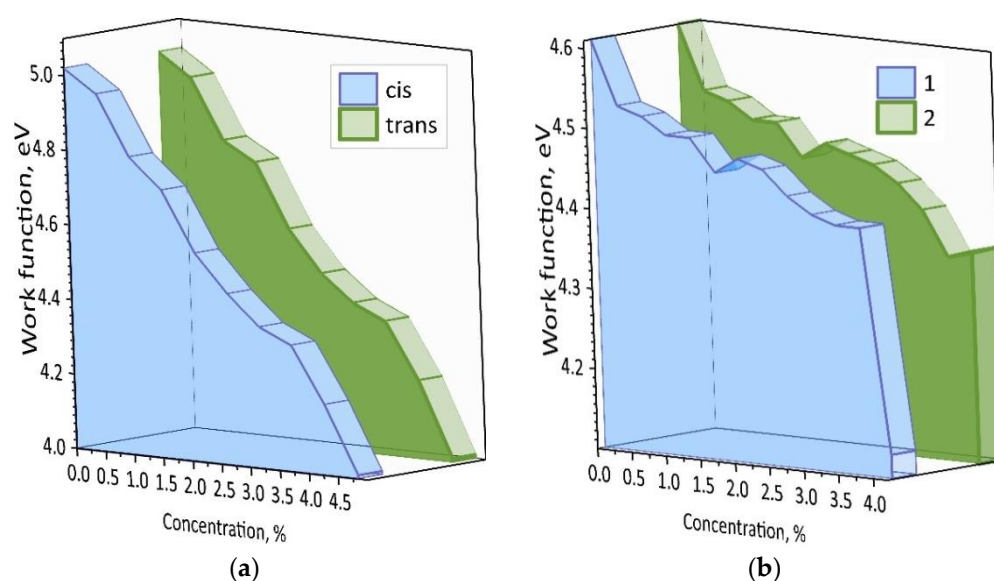


**Figure 5.** Fragments of the supercell with 12 amine groups in two options: before (**left**) and after optimization (**right**).

**Table 3.** Energetic parameters of functionalized graphene.

| $C_{NH2}$, % | NH$_2$ | ΔE, eV | E$_F$, eV | E$_{gap}$, eV | NH$_2$ | ΔE, eV | E$_F$, eV | E$_{gap}$, eV |
|---|---|---|---|---|---|---|---|---|
| 2.78 | 8-1 | −1.62 | −4.41 | 0.06 | 8-2 | −1.61 | −4.43 | 0.06 |
| 3.13 | 9-1 | −1.37 | −4.39 | 0.06 | 9-2 | −1.29 | −4.41 | 0.06 |
| 3.47 | 10-1 | −2.53 | −4.38 | 0.07 | 10-2 | −1.55 | −4.37 | 0.07 |
| 3.82 | 11-1 | −0.92 | −4.38 | 0.07 | 11-2 | −1.32 | −4.32 | 0.07 |
| 4.17 | 12-1 | 1.74 | −4.09 | 0.07 | 12-2 | −0.17 | −4.33 | 0.07 |

Based on the performed calculations, the dependence of the work function on the amine group concentration in the graphene and GNM was obtained (Figure 6). In both cases, with increasing concentration, the work function gradually decreases (in the case of GNM from 5 eV to 4 eV).



**Figure 6.** The dependence of work function on the concentration of amino groups in (**a**) nanoscale graphene; (**b**) basal surface of graphene.

*3.3. Experimental Characterization*

The acquired theoretical data on the functionalization limit of the holey and intact graphene by the amine groups and their effect on the material's work function are well-supported by our experimental findings. Using wet-chemistry protocols, the holey and intact Am graphene were synthesized and examined by core-level techniques to assess the maximum concentration of the introduced amines in each case. Samples from five consecutive syntheses for each type of Am graphene were studied with the acquired data processed and averaged to acquire statistically relevant results. Figure 7 displays exemplar X-ray photoelectron spectra of the C-ny graphene prior to and after the applied amination (Am#1). The C-ny graphene has a perforated structure with a matrice of 2–4 nm holes in diameter [42], whereas the abundance of the edge-located ketone groups with the negligible amount of other reactive oxygen groups ensures amination occurs only at the edges of the nanoscale holes, not on the basal plane. As a net result, aminated C-ny graphene corresponds well to the simulated holey Am graphene layer.
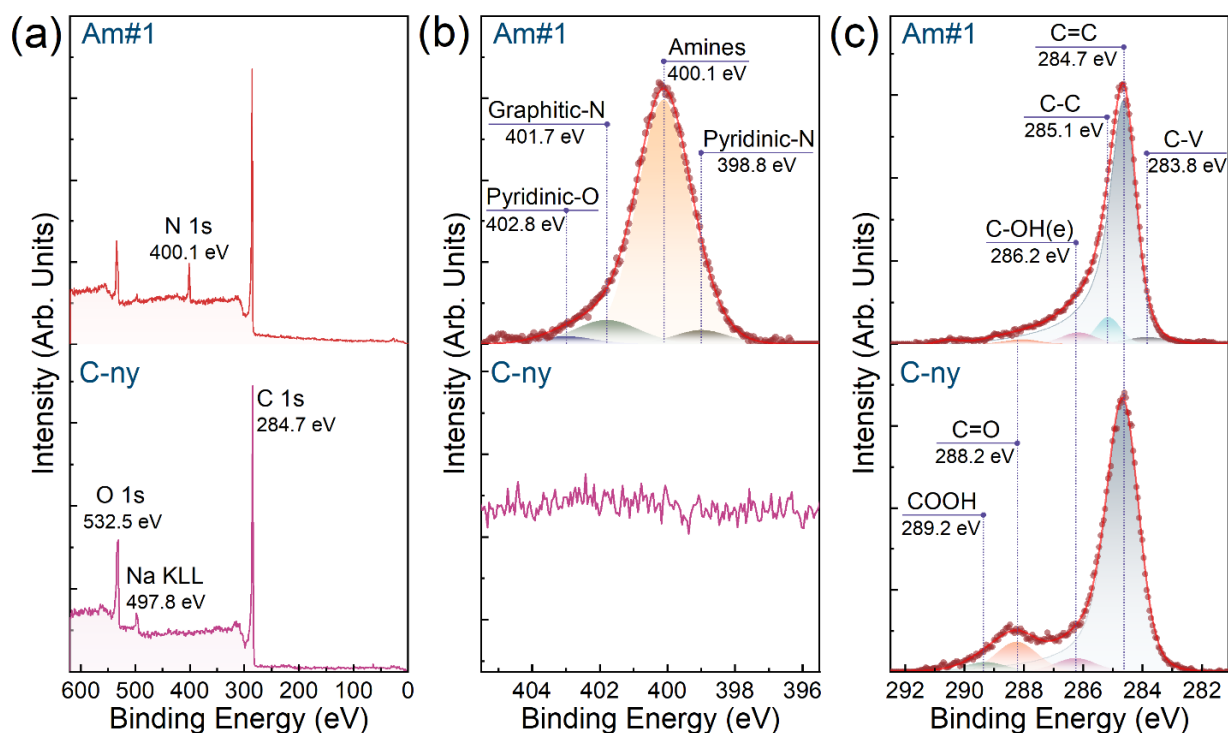
**Figure 7.** Characterization of the chemistry in the considered C-ny graphene and Holey Am layer (Am#1) via XPS. (**a**) Survey spectra, (**b**) high-resolution N 1*s* spectra, and (**c**) high-resolution C 1*s* spectra.

According to the acquired survey spectra (Figure 7a), upon the applied amination the O 1*s* line with the binding energy (*BE*) of 532.5 eV substantially diminished, while the N 1*s* peak with the *BE* of 400.1 eV appeared [47], pointing out the successful introduction of the nitrogen-containing functionalities. The concentration of nitrogen was estimated to be 5.73 at.%. To further analyze the composition of nitrogen-containing groups embedded upon the applied treatment, high-resolution N 1*s* spectra were acquired and processed, shown in Figure 7b. Four peaks were discerned in the N 1*s* spectrum of Am#1 with *BE*s of 400.1 eV, 398.8 eV, 401.7 eV, 402.8 eV, which are related to amines, pyridines, graphitic nitrogen and pyridine-N-oxide moieties introduced into the graphene layer, respectively [47–49]. Amines are demonstrated to be the dominant form of the nitrogen groups with the relative content estimated to be up to 82.8%. Accordingly, the highest achieved concentration of the introduced amines is 4.74 at.%, which coincides well with the theoretical data (Table 1).

Notably, this value is several times lower than the concentration of the ketone groups in the initial C-ny graphene, which are being substituted during the applied amination process. Prior to the amination, a distinguishable peak with the BE of 288.2 eV related to the ketone groups is discerned in the C-ny graphene C 1*s* spectrum [49,50], which is displayed in Figure 7c. The concentration of ketones derived from the deconvoluted C 1*s* spectrum is estimated to be equal to 9.89 at.%, while after the amination this value drastically diminishes down to 0.71 at.% with the corresponding peak being hardly distinguished. This implies that upon the applied amination, the maximum number of amines has been introduced with the retained ketones being just eliminated or substituted by a minor number of other nitrogen-containing functionalities. Thus, the acquired experimental data on the holey aminated graphene ratify the theoretically determined threshold quantity of the amines introduced to the holey graphene of ca. 4.8 at.%

Moving to the threshold quantity of the amines on the intact graphene, which are the basal-plane amines, the pristine GO was aminated according to the same procedure as for the C-ny graphene. Figure 8 displays the XPS data on the GO prior to and after being aminated at two different reaction temperatures of 125 °C (Am#2) and 165 °C (Am#3) in

otherwise identical conditions. Compared to the C-ny graphene, GO is predominantly functionalized by the basal-plane hydroxyls and epoxides as seen from the GO C 1*s* spectrum in Figure 8a, with the corresponding peak at BE of 286.8 eV being dominant [51]. The estimated concentration of hydroxyls and epoxides is 38.4 at.%. Upon the applied reductive amination, these moieties are substituted with the introduction of the basal-plane amines or otherwise just eliminated if the amine group cannot be covalently bonded to the graphene layer. This fact is signified by the almost complete absence of the C-OH&C-O-C peak in the C 1*s* spectra of Am#2 and Am#3 spectra with the appearance of the N 1*s* spectral line in the survey spectra (Figure 8b) of these samples. The derived concentrations of the nitrogen-containing functionalities in the Am#2 and Am#3 samples are 5.36 at.% and 8.74 at.%, respectively, with the second value more than two times exceeding the threshold determined from the theoretical calculations. However, the thorough examination of the N 1*s* spectra displayed in Figure 8c points out that this fact is related to the rise of the relative concentration of pyridines, which ratio increases from 4.28% to 39.94%. At the same time, the relative concentration of the amines drops from 87.18% to 56.04% with the corresponding values of the atomic concentration of 4.67 at.% and 4.89 at.%, respectively. These results emphasize that the threshold quantity of the amines on the basal plane of the graphene is of 4.7–4.9 at.%, which is in good consistency with the performed theoretical calculations. In turn, the maximization of the nitrogen concentration by varying the synthesis parameters results not in the boost in the number of amines, but the introduction of other nitrogen-containing moieties, particularly pyridines.
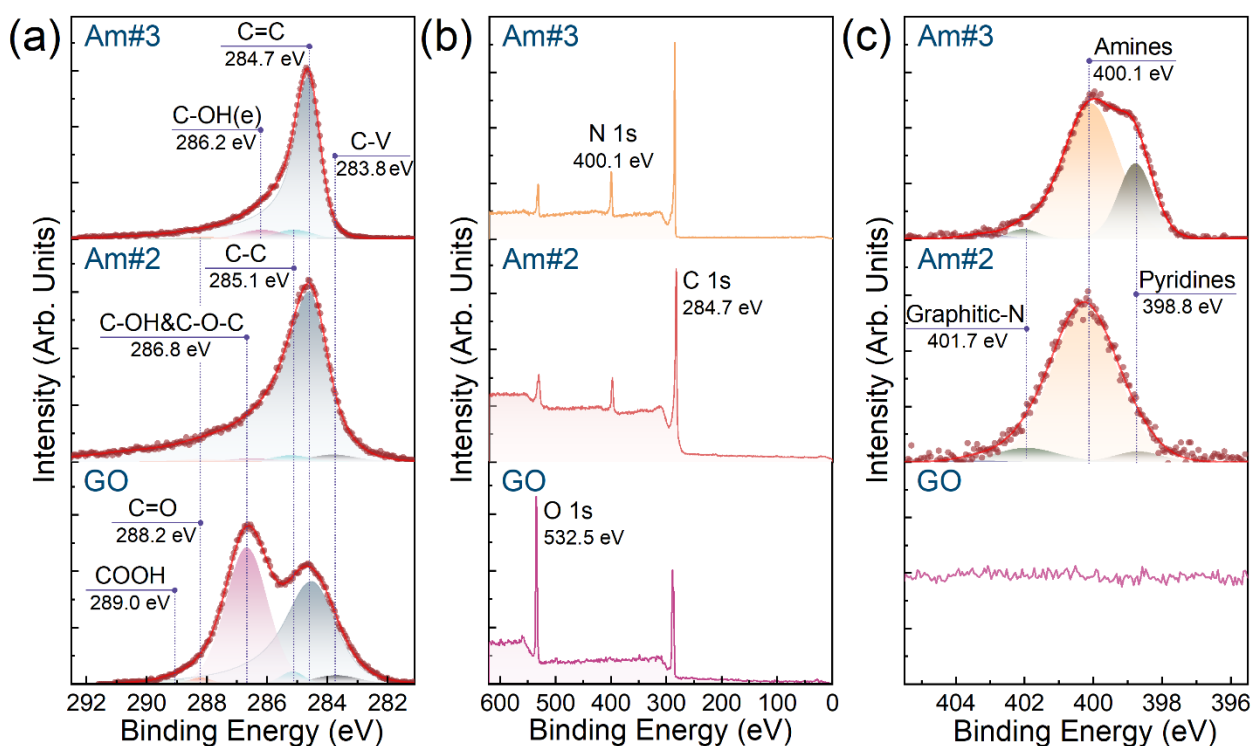


**Figure 8.** XPS characterization of the chemistry in the initial GO and Am layers synthesized at different temperatures (Am#2 and Am#3). (**a**) High-resolution C 1*s* spectra, (**b**) survey spectra, and (**c**) high-resolution N 1*s* spectra.

The introduction of pyridines and other heterocyclic nitrogen-containing moieties instead of amines is additionally reflected by the microscopic studies on the morphology of Am#2 and Am#3 layers. Figure 9a,b display the TEM images and the ED patterns of the considered GO, Am#2 and Am#3 layers. As can be seen, upon moving from the Am#2 to Am#3 with the increase in the nitrogen concentration, distinguishable nanoscale holes (black dots indicated by arrows) appear, with the diffraction maxima becoming blurred due

to the deviations in the angle between the electronic beam and graphene surface [52]. This is in contrast to the intact Am#2 and GO layers with no observable nanoscale defects and the preservation of the sharp diffraction maxima in the ED pattern. Thus, the persistent implementation of nitrogen-containing groups results in the disruption of the graphene layer, as is demonstrated by the theoretical simulations with the subsequent formation of the heterocyclic moieties.
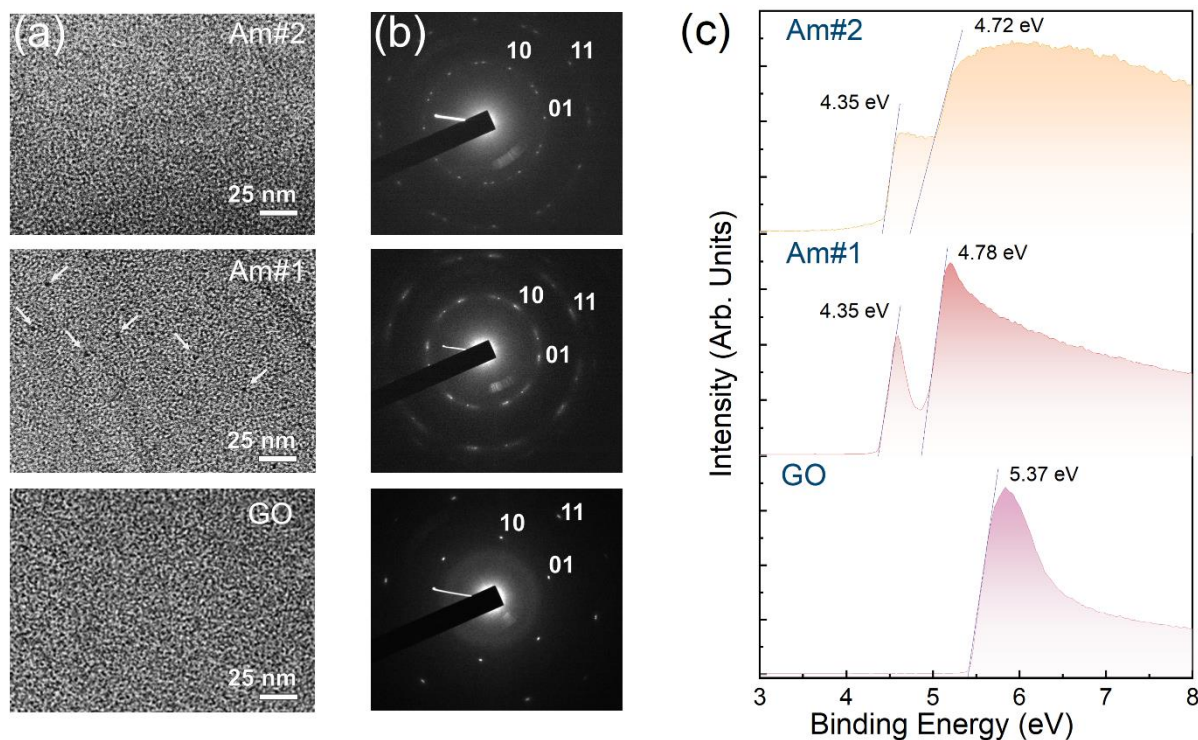


**Figure 9.** Characterization of the initial GO and Am layers' morphology and electronic properties. (**a**) TEM images, (**b**) ED patterns, and (**c**) Cut-off SE spectra of the materials under study.

To finally validate the theoretically predicted reduction of the WF value upon the amination of the graphene layer, the SE spectra of the GO, Am#1 and Am#2 samples were collected, which are displayed in Figure 9c. The SE spectrum of GO is presented by a single maximum with the marked cut-off threshold (dashed lines) of 5.37 eV, well-consistent with the published data on the WF value of GO [53]. In turn, the SE spectra of Am#1 and Am#2 samples exhibit a more complicated nature with two slopes and the corresponding WF values of 4.72–4.78 eV and 4.35 eV. Such a shape of the SE spectra implies separation of the graphene layer in two different areas, which can be regarded as areas of the pristine graphene network and its local areas functionalized with amines. This hint is supported by the fact that the first WF value coincides with the reported ones for the reduced GO [53,54], whereas the presence of amines was demonstrated to reduce the WF of the graphene layer [54]. Thus, collectively with the theoretical calculations, the experimental studies indicate that the introduction of the amine groups reduces the WF value of graphene, although this is related to local areas of the material, not the whole layer.

## 4. Conclusions

With the help of in silico studies, the maximum possible concentration of amine groups on the graphene nanomesh was established on holes—4.8 at.%. This is exactly the maximum concentration, since the supercell for research was chosen as the minimum of all possible options—with a minimum diameter hole of ~1.2 nm and a minimum width neck of ~1 nm. For the basal surface of graphene, the mechanism of functionalization by the amine groups was studied. It was found that no more than 11 groups can be deposited and

covalently bound to graphene in one local area. With further functionalization, the amine groups break the graphene layer.

The performed experimental studies well-supported our theoretical results on the threshold quantity of the amines both in the holey and intact graphene, giving a comparable value of 4.6–4.8 at.% of the introduced amines and indicating that a further increase in the content of the nitrogen-containing groups is related to the implementation of the hetero-cyclic moieties due to the disruption of the graphene layer. Furthermore, the predicted reduction of the WF value is demonstrated experimentally, although with a hint that such a reduction is of a local nature.

**Conflicts of Interest:** The authors declare no conflict of interest.

# References

1. Lokhande, A.C.; Qattan, I.A.; Lokhande, C.D.; Patole, S.P. Holey graphene: An emerging versatile material. *J. Mater. Chem. A* **2020**, *8*, 918–977. [CrossRef]
2. Lin, Y.; Liao, Y.; Chen, Z.; Connell, J.W. Holey graphene: A unique structural derivative of graphene. *Mater. Res. Lett.* **2017**, *5*, 209–234.
3. Liu, T.; Zhang, L.; Cheng, B.; Hu, X.; Yu, J. Holey Graphene for Electrochemical Energy Storage. *Cell Rep. Phys. Sci.* **2020**, *1*, 100215. [CrossRef]
4. Zhang, J.; Song, H.; Zeng, D.; Wang, H.; Qin, Z.; Xu, K.; Pang, A.; Xie, C. Facile synthesis of diverse graphene nanomeshes based on simultaneous regulation of pore size and surface structure. *Sci. Rep.* **2016**, *6*, 32310. [CrossRef]
5. Yuan, W.; Li, M.; Wen, Z.; Sun, Y.; Ruan, D.; Zhang, Z.; Chen, G.; Gao, Y. The Fabrication of Large-Area, Uniform Graphene Nanomeshes for High-Speed, Room-Temperature Direct Terahertz Detection. *Nanoscale Res. Lett.* **2018**, *13*, 190. [CrossRef] [PubMed]
6. Han, T.H.; Huang, Y.-K.; Tan, A.T.L.; Dravid, V.P.; Huang, J. Steam Etched Porous Graphene Oxide Network for Chemical Sensing. *Am. Chem. Soc.* **2011**, *133*, 15264–15267. [CrossRef] [PubMed]
7. Ning, G.; Fan, Z.; Wang, G.; Gao, J.; Qian, W.; Wei, F. Gram-scale synthesis of nanomesh graphene with high surface area and its application in supercapacitor electrodes. *Chem. Commun.* **2011**, *47*, 5976–5978. [CrossRef]
8. Peng, W.; Liu, S.; Sun, H.; Yao, Y.; Zhi, L.; Wang, S. Synthesis of porous reduced graphene oxide as metal-free carbon for adsorption and catalytic oxidation of organics in water. *Mater. Chem. A* **2013**, *1*, 5854–5859. [CrossRef]
9. Han, X.; Funk, M.R.; Shen, F.; Chen, Y.-C.; Li, Y.; Campbell, C.J.; Dai, J.; Yang, X.; Kim, J.-W.; Liao, Y.; et al. Scalable Holey Graphene Synthesis and Dense Electrode Fabrication toward High-Performance Ultracapacitors. *ACS Nano* **2014**, *8*, 8255–8265. [CrossRef]
10. Esfandiar, A.; Kybert, N.J.; Dattoli, E.N.; Han, G.H.; Lerner, M.B.; Akhavan, O.; Irajizad, A.; Charlie Johnson, A.T. DNA-decorated graphene nanomesh for detection of chemical vapors. *Appl. Phys. Lett.* **2013**, *103*, 183110. [CrossRef]
11. Chen, Z.; Zhang, Y.; Yang, Y.; Shi, X.; Zhang, L.; Jia, G. Hierarchical nitrogen-doped holey graphene as sensitive electrochemical sensor for methyl parathion detection. *Sens. Actuators B Chem.* **2021**, *336*, 129721. [CrossRef]
12. Jiang, Z.; Jiang, Z.-J.; Tiana, X.; Chen, W. Amine-functionalized holey graphene as a highly active metal-free catalyst for the oxygen reduction reaction. *J. Mater. Chem. A* **2014**, *2*, 441–450. [CrossRef]

13. Zhao, X.; Hayner, C.M.; Kung, M.C.; Kung, H.H. In-Plane Vacancy-Enabled High-Power Si–Graphene Composite Electrode for Lithium-Ion Batteries. *Adv. Energy Mater.* **2011**, *1*, 1079–1084. [CrossRef]
14. Xu, J.; Lin, Y.; Connell, J.W.; Dai, L. Nitrogen-Doped Holey Graphene as an Anode for Lithium-Ion Batteries with High Volumetric Energy Density and Long Cycle Life. *Small* **2015**, *11*, 6179–6185. [CrossRef]
15. Wang, X.; Yang, Y.; Zhang, Q.; Yang, X.; Hu, Z. Lamellar Oxygen-Enriched Graphene Hydrogel with Linking-up Network Porous Structure for High-Performance Supercapacitors. *J. Phys. Chem. C* **2018**, *122*, 6526–6538. [CrossRef]
16. Xu, Y.; Fan, B.; Liu, Z.; Huang, C.; Hu, A.; Tang, Q.; Zhang, S.; Deng, W.; Chen, X. Redox-active engineered holey reduced graphene oxide films for K+ storage. *Carbon* **2021**, *174*, 173–179. [CrossRef]
17. Zakaria, A.B.M.; Vasquez, E.S.; Walters, K.B.; Leszczynska, D. Functional holey graphene oxide: A new electrochemically transformed substrate material for dopamine sensing. *RSC Adv.* **2015**, *5*, 107123–107135. [CrossRef]
18. Huang, J.-B.; Patra, J.; Lin, M.-H.; Ger, M.-D.; Liu, Y.-M.; Pu, N.-W.; Hsieh, C.-T.; Youh, M.-J.; Dong, Q.-F.; Chang, J.-K. A Holey Graphene Additive for Boosting Performance of Electric Double-Layer Supercapacitors. *Polymers* **2020**, *12*, 765. [CrossRef]
19. Lin, Y.; Han, X.; Campbell, C.J.; Kim, J.-W.; Zhao, B.; Luo, W.; Dai, J.; Hu, L.; Connell, J.W. Holey Graphene Nanomanufacturing: Structure, Composition, and Electrochemical Properties. *Adv. Funct. Mater.* **2015**, *25*, 2920–2927. [CrossRef]
20. Yang, M.; Wang, Y.; Dong, L.; Xu, Z.; Liu, Y.; Hu, N.; Kong, E.S.-W.; Zhao, J.; Peng, C. Gas Sensors Based on Chemically Reduced Holey Graphene Oxide Thin Films. *Nanoscale Res. Lett.* **2019**, *14*, 218. [CrossRef]
21. Ziółkowski, R.; Górski, Ł.; Malinowska, E. Carboxylated graphene as a sensing material for electrochemical uranyl ion detection. *Sens. Actuators B* **2017**, *238*, 540–547. [CrossRef]
22. Marsden, A.J.; Brommer, P.; Mudd, J.J.; Dyson, M.A.; Cook, R.; Asensio, M.; Avila, J.; Levy, A.; Sloan, J.; Quigley, D.; et al. Effect of oxygen and nitrogen functionalization on the physical and electronic structure of graphene. *Nano Res.* **2015**, *8*, 2620–2635. [CrossRef]
23. Suvarnaphaet, P.; Pechprasarn, S. Graphene-Based Materials for Biosensors: A Review. *Sensors* **2017**, *17*, 2161. [CrossRef] [PubMed]
24. Valentini, L.; Cardinali, M.; Bittolo Bon, S.; Bagnis, D.; Verdejo, R.; Lopez-Manchado, M.A.; Kenny, J.M. Use of butylamine modified graphene sheets in polymer solar cells. *J. Mater. Chem.* **2010**, *20*, 995–1000. [CrossRef]
25. Zhang, W.; Ma, J.; Gao, D.-G.; Zhou, Y.; Li, C.; Zha, J.; Zhang, J. Preparation of amino-functionalized graphene oxide by Hoffman rearrangement and its performances on polyacrylate coating latex. *Prog. Org. Coat.* **2016**, *94*, 9–17. [CrossRef]
26. Krasteva, N.; Keremidarska-Markova, M.; Hristova-Panusheva, K.; Andreeva, T.; Speranza, G.; Wang, D.; Draganova-Filipova, M.; Miloshev, G.; Georgieva, M. Aminated Graphene Oxide as a Potential New Therapy for Colorectal Cancer. *Oxid. Med. Cell Longev.* **2019**, *2019*, 3738980. [CrossRef]
27. Baraket, M.; Stine, R.; Lee, W.K.; Robinson, J.T.; Tamanaha, C.R.; Sheehan, P.E.; Walton, S.G. Aminated graphene for DNA attachment produced via plasma functionalization. *Appl. Phys. Lett.* **2012**, *100*, 233123. [CrossRef]
28. Boukhvalov, D.W. DFT modeling of the covalent functionalization of graphene: From ideal to realistic models. *RSC Adv.* **2013**, *3*, 7150–7159. [CrossRef]
29. Boukhvalov, D.W.; Katsnelson, M.I. Chemical functionalization of graphene. *J. Phys. Condens. Matter* **2009**, *21*, 344205. [CrossRef]
30. Boukhvalov, D.W.; Son, Y.-W. Oxygen reduction reactions on pure and nitrogen-doped graphene: A first-principles modeling. *Nanoscale* **2012**, *4*, 417. [CrossRef]
31. Wang, M.C.; Lai, Z.B.; Galpaya, D.; Yan, C.; Hu, N.; Zhou, L.M. Atomistic simulation of surface functionalization on the interfacial properties of graphene-polymer nanocomposites. *J. Appl. Phys.* **2014**, *115*, 123520. [CrossRef]
32. Al Mahmud, H.; Radue, M.S.; Pisani, W.A.; Odegard, G.M. Computational Modeling of Hybrid Carbon Fiber/Epoxy Composites Reinforced with Functionalized and Non-Functionalized Graphene Nanoplatelets. *Nanomaterials* **2021**, *11*, 2919. [CrossRef] [PubMed]
33. Sinclair, R.C.; Coveney, P.V. Modeling Nanostructure in Graphene Oxide: Inhomogeneity and the Percolation Threshold. *J. Chem. Inf. Model.* **2019**, *59*, 2741–2745. [CrossRef] [PubMed]
34. Lerf, A.; He, H.; Forster, M.; Klinowski, J. Structure of Graphite Oxide Revisited. *J. Phys. Chem. B* **1998**, *102*, 4477–4482. [CrossRef]
35. Aliyev, E.; Filiz, V.; Khan, M.M.; Lee, Y.J.; Abetz, C.; Abetz, V. Structural Characterization of Graphene Oxide: Surface Functional Groups and Fractionated Oxidative Debris. *Nanomaterials* **2019**, *9*, 1180. [CrossRef] [PubMed]
36. Dreyer, D.R.; Park, S.; Bielawski, C.W.; Ruo, R.S. The chemistry of graphene oxide. *Chem. Soc. Rev.* **2010**, *39*, 228–240. [CrossRef]
37. Xu, Y.; Shi, G. Assembly of chemically modified graphene: Methods and applications. *J. Mater. Chem.* **2011**, *21*, 3311–3323. [CrossRef]
38. Eigler, S.; Hirsch, A. Chemistry with Graphene and Graphene Oxide—Challenges for Synthetic Chemists. *Angew. Chem. Int. Ed.* **2014**, *53*, 2–21. [CrossRef]
39. Rabchinskii, M.K.; Ryzhkov, S.A.; Kirilenko, D.A.; Ulin, N.V.; Baidakova, M.V.; Shnitov, V.V.; Pavlov, S.I.; Chumakov, R.G.; Stolyarova, D.Y.; Besedina, N.A.; et al. From graphene oxide towards aminated graphene: Facile synthesis, its structure and electronic properties. *Sci. Rep.* **2020**, *10*, 6902. [CrossRef]
40. Elstner, M.; Porezag, D.; Jungnickel, G.; Elsner, J.; Haugk, M.; Frauenheim, T.; Suhai, S.; Seifert, G. Self-consistent-charge density-functional tight-binding method for simulations of complex materials properties. *Phys. Rev. B* **1998**, *58*, 7260–7268. [CrossRef]

41. Hourahine, B.; Aradi, B.; Blum, V.; Bonafé, F.; Buccheri, A.; Camacho, C.; Cevallos, C.; Deshaye, M.Y.; Dumitrică, T.; Dominguez, A.; et al. DFTB+, a software package for efficient approximate density functional theory based atomistic simulations. *J. Chem. Phys.* **2020**, *152*, 124101. [CrossRef] [PubMed]

42. Rabchinskii, M.K.; Varezhnikov, A.S.; Sysoev, V.V.; Solomatin, M.A.; Ryzhkov, S.A.; Baidakova, M.V.; Stolyarova, D.Y.; Shnitov, V.V.; Pavlov, S.S.; Kirilenko, D.A.; et al. Hole-matrixed carbonylated graphene: Synthesis, properties, and highly-selective ammonia gas sensing. *Carbon* **2021**, *172*, 236–247. [CrossRef]

43. Aguilar-Bolados, H.; Vargas-Astudillo, D.; Yazdani-Pedram, M.; Acosta-Villavicencio, G.; Fuentealba, P.; Contreras-Cid, A.; Verdejo, R.; López-Manchado, M.A. Facile and Scalable One-Step Method for Amination of Graphene Using Leuckart Reaction. *Chem. Mater.* **2017**, *29*, 6698–6705. [CrossRef]

44. Molodtsov, S.L.; Fedoseenko, S.I.; Vyalikh, D.V.; Iossifov, I.E.; Follath, R.; Gorovikov, S.A.; Brzhezinskaya, M.M.; Dedkov, Y.S.; Püttner, R.; Schmidt, J.-S.; et al. High-resolution Russian–German beamline at BESSY. *Appl. Phys. A* **2009**, *94*, 501–505. [CrossRef]

45. Helander, M.G.; Greiner, M.T.; Wang, Z.B.; Lu, Z.H. Pitfalls in measuring work function using photoelectron spectroscopy. *Appl. Surf. Sci.* **2010**, *256*, 2602–2605. [CrossRef]

46. Glukhova, O.E.; Barkov, P.V. A new method for determining energetically favorable landing sites of carboxyl groups during functionalization of graphene nanomesh. *Lett. Mater.* **2021**, *12*, 392–396. [CrossRef]

47. Rabchinskii, M.K.; Saveliev, S.D.; Stolyarova, D.Y.; Brzhezinskaya, M.; Kirilenko, D.A.; Baidakova, M.V.; Ryzhkov, S.A.; Shnitov, V.V.; Sysoev, V.V.; Brunkov, P.N. Modulating nitrogen species via N-doping and post annealing of graphene derivatives: XPS and XAS examination. *Carbon* **2021**, *182*, 593–604. [CrossRef]

48. Rabchinskii, M.K.; Ryzhkov, S.A.; Gudkov, M.V.; Baidakova, M.V.; Saveliev, S.D.; Pavlov, S.I.; Shnitov, V.V.; Kirilenko, D.A.; Stolyarova, D.Y.; Lebedev, A.M.; et al. Unveiling a facile approach for large-scale synthesis of N-doped graphene with tuned electrical properties. *2D Mater.* **2020**, *7*, 045001. [CrossRef]

49. Schultz, B.J.; Dennis, R.V.; Aldinger, J.P.; Jaye, C.; Wang, X.; Fischer, D.A.; Cartwright, A.N.; Banerjee, S. X-ray absorption spectroscopy studies of electronic structure recovery and nitrogen local structure upon thermal reduction of graphene oxide in an ammonia environment. *RSC Adv.* **2014**, *4*, 634–644. [CrossRef]

50. Shnitov, V.V.; Rabchinskii, M.K.; Brzhezinskaya, M.; Stolyarova, D.Y.; Pavlov, S.V.; Baidakova, M.V.; Shvidchenko, A.V.; Kislenko, V.A.; Kislenko, S.A.; Brunkov, P.N. Valence Band Structure Engineering in Graphene Derivatives. *Small* **2021**, *17*, 2104316. [CrossRef]

51. Ganguly, A.; Sharma, S.; Papakonstantinou, P.; Hamilton, J. Probing the thermal deoxygenation of graphene oxide using high-resolution in situ X-ray-based spectroscopies. *J. Phys. Chem. C* **2011**, *115*, 17009–17019. [CrossRef]

52. Kirilenko, D.A.; Dideykin, A.T.; Van Tendeloo, G. Measuring the corrugation amplitude of suspended and supported graphene. *Phys. Rev. B* **2011**, *84*, 235417. [CrossRef]

53. Kang, B.; Lim, S.; Lee, W.H.; Jo, S.B.; Cho, K. Work-Function-Tuned Reduced Graphene Oxide via Direct Surface Functionalization as Source/Drain Electrodes in Bottom-Contact Organic Transistors. *Adv. Mater.* **2013**, *25*, 5856–5862. [CrossRef]

54. Ji, S.; Min, B.K.; Kim, S.K.; Myung, S.; Kang, M.; Shin, H.-S.; Song, W.; Heo, J.; Lim, J.; An, K.-S.; et al. Work function engineering of graphene oxide via covalent functionalization for organic field-effect transistors. *Appl. Surf. Sci.* **2017**, *419*, 252–258. [CrossRef]